Article

Co-Encapsulation of Rhenium and Ruthenium Complexes into the Scaffolds of Metal–Organic Framework to Promote CO$_2$ Reduction

Zhifang Su, Baolan Yu, Jianxin Feng, Maoling Zhong, Xuan Li and Jianying Shi *

School of Chemistry, LIFM, IGCME, Sun Yat-Sen University, Guangzhou 510275, China
* Correspondence: shijying@mail.sysu.edu.cn

Abstract: The molecular complexes of Re(4,4′-dcbpy)(CO)$_3$Cl (dcbpy = dicarboxylicacid-2,2′-bipyridyl) and [Ru(dcbpy)$_3$]$^{2+}$ are co-assembled into UiO-66 scaffolds as structural imperfects for CO$_2$ photocatalytic reduction (named as Re-Ru@U). The prepared catalysts are characterized by XRD, Fourier-Transform infrared (FTIR) spectra, X-ray photoelectron spectra (XPS) and N$_2$ adsorption–desorption isotherms. The intact structure of molecular complexes within the matrix are monitored by ^{1}H nuclear magnetic resonance (NMR) spectra through a totally digesting catalyst. The optical properties are studied via absorption and photoluminescence spectra, and the single-electron reduction in Re and Ru complexes is detected by electron paramagnetic resonance (EPR) spectra. An excellent photocatalytic performance is obtained with steady and sustained CO evolution and a turnover number (TON) value of 15 (11 h). The CO activity irradiating by single wavelength presents the absorption-intensity-dependent changing tendency, where the absorption intensity is superposed by Re and Ru complexes. The two radicals related to Re and Ru, respectively, are simultaneously detected in the Re-Ru@U catalyst. It is suggested that the ReC$_2$ component serves as both a photosensitizer and a catalyst, and the RuC$_2$ component works as an additional photosensitizer to supply the second electron for CO$_2$ reduction. The co-assembling of dual metals Re and Ru in the matrix promotes the electron transfer from the reductive Ru centres to one-electron-reduced Re centres and accounts for the superior activity of CO evolution. Our results demonstrate a strategy to develop the multimetallic catalysts via facile assembling into MOF scaffolds to promote photocatalytic performance.

Keywords: rhenium; ruthenium; CO$_2$ reduction; electron communication

1. Introduction

Solar-light-driven CO$_2$ reduction is a promising route to fulfil the conversion of sustainable solar energy to chemical energy stored into chemical bonds [1,2]. The molecule-based photosystems composed of the photosensitizers, catalytic centres and the electron relays have been widely investigated in artificial photosynthesis [3–6]. For improving the overall catalytic efficiency, the covalently or co-ordinately linking the photosensitive units and the catalytic units into a single-component multinuclear complex is carried out to promote the electron transfer between photosensitizers and catalytic centres [7–10]. However, the multimetallic assemblies are somewhat impractical as complicated synthetic processes. Furthermore, the absence of sustainability for molecular complexes under harsh reaction conditions remains an ongoing challenge [8,11,12].

Hierarchically, co-organizing light-harvesting chromophores and catalytic centres into metal–organic frameworks (MOFs) [13] and crystalline porous materials constituted by metal ions/clusters and organic linkers is a competent way to assemble photosensitizers and catalysts instead of covalently linking them [14]. Additionally, integrating molecular complexes into MOFs supports could maintain homogenous catalytic activity, meanwhile imparting heterogenous stability [9,13–18]. In our previous works, a universal strategy of "bottle-around-a-ship" was developed to assemble molecular complexes into MOFs'

scaffolds through the improper coordination between MOF nodes and/or organic linkers with molecular complexes, concomitantly generating the structural imperfects around these mismatch sites [19–21]. The atomically precise $Au_{25}(SG)_{18}$ and metal–organic cage (MOC) of $[Pd_6(RuL_3)_8]^{28+}$ (MOC-16) had been successfully encapsulated into MOFs' scaffolds of ZIF-8 and/or UiO-66 with their high tolerances to structural defects [19–21].

As a star of molecular catalysts to convert CO_2 with exclusive CO selectivity, rhenium diimine carbonyl molecule catalysts were studied in our reported work [22], where rhenium complexes were encapsulated into ZIF-8 and UiO-66 matrixes with different host–guest interactions. The different microenvironments of Re complexes in ZIF-8 and UiO-66 matrixes diverted the CO_2 activation pathway and engendered the disparity for CO evolution in Re@ZIF-8 and Re@UiO-66. The inferior photocatalytic activity in Re@UiO-66 demonstrated that the solvation shell surrounding Re complexes delayed the electron transfer between Re complexes inside the UiO-66 matrix and electron donors in solution. Notably, in these two cases, the site-isolated Re complex had to serve as duel identities of a photosensitizer and an active catalyst for the photoreduction in CO_2 [22]. In comparison with the reported dual-metal system with Re and Ru complexes, such as co-incorporated Ru-MOF-253-Re and impregnated ReRu-66 on the surface of UiO-66 [23,24], the performance of Re complexes in the UiO-66 matrix still has potential for improvement by introducing additional Ru complex photosensitizers. In addition, the co-assembling of Re and Ru complexes into MOFs provides a model system to disclose the electron communication between Re and Ru complexes within the porous matrix.

Herein, $Re(4,4'$-dcbpy$)(CO)_3Cl$ (dcbpy = dicarboxylicacid-2,2′-bipyridyl) (ReC_2) and $[Ru(dcbpy)_3]^{2+}$ (RuC_6) complexes are concurrently incorporated into UiO-66, named as Re-Ru@U, with incompatible molecular sizes (12 Å and 15 Å) to the pore sizes of UiO-66 (~8.0 Å and ~11.0 Å) [24,25]. The Re-Ru@U catalyst presents the excellent activity and durability for CO_2 photocatalytic reduction, in comparison with control samples of single metal complex catalysts, free in homogenous solution or stuck in the heterogeneous UiO-66 matrix. Specifically, the superior activity observed in Re-Ru@U is discussed in view of the possible electron transfer between Ru centres and Re centres.

2. Results and Discussion

2.1. Synthetic Strategy

The Re-Ru@U photocatalyst was synthesized by the coordinating-assembly strategy developed in our previous works [19–21]. In detail, ReC_2 and RuC_6 complexes with the default ratio were mixed with the preforming Zr-oxo clusters to allow for the appended carboxylic group on metal complexes, coordinating to the Zr-oxo clusters in a mono- or bidentate fashion. In the following step, 1,4-benzenedicarboxylate (BDC) linkers are added to coordinate with the Zr-oxo clusters to grow the UiO-66 matrix, during which, both ReC_2 and RuC_6 complexes are encapsulated into the scaffolds to engender the imperfect structure. A series of samples with different ratios of Ru to Re were prepared, and the dosages of ReC_2 and RuC_6 were optimized by CO_2 reduction performance listed in Table S1. The composition of ReC_2 and RuC_6 in Re-Ru@U determined by inductively coupled plasma mass spectra (ICP-MS) is 2.45 wt% and 0.11 wt%, respectively. As control, ReC_2 and RuC_6 complexes were separately integrated into the UiO-66 matrix with the equivalent amount to that of Re-Ru@U, denoted as Re@U and Ru@U. Meanwhile, the ReC_2 and RuC_6 complexes were co-impregnated on the surface of the UiO-66 matrix, named as Re-Ru/U.

2.2. Structure Characterizations

The structures of as-synthesized Re-Ru@U, Re@U, Ru@U and UiO-66 are characterized by powder X-ray diffraction (PXRD) and FT-IR, as shown in Figure S1. The diffraction patterns of Re-Ru@U, Re@U and Ru@U match well with the peaks of pristine UiO-66 [26], indicating their crystalline nature with the integration of metal complexes into scaffolds. In the IR spectra, the featured IR bands related to carbonyl asymmetric vibration at 2026, 1924 and 1910 cm^{-1} are observed for the Re-contained catalysts of Re@U and Re-Ru@U [27,28],

indicating the incorporation of ReC_2 into the UiO-66 matrix. The uniform dispersion of Re and Ru complexes inside the UiO-66 matrix without aggregation is verified by the representative aberration-corrected high-angle annular dark-field (HAADF) scanning transmission electron microscopy (STEM) images and the energy-dispersive X-ray (EDX) spectroscopy element mapping, as shown in Figure 1.
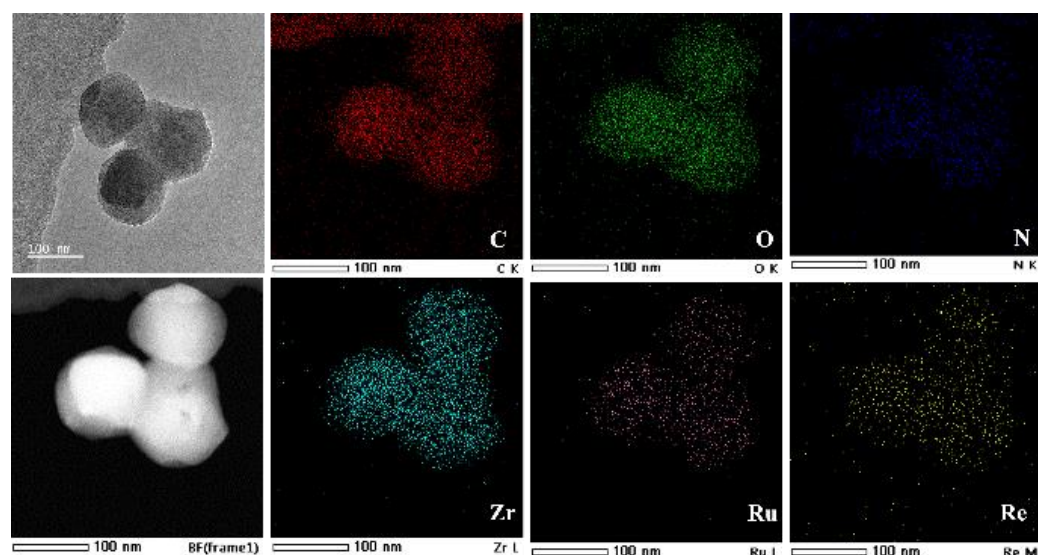

Figure 1. HAADF-STEM images and corresponding EDX spectrum of Re-Ru@U.

The incorporation of Re and Ru into the UiO-66 matrix was further confirmed by the binding energy (BE) in X-ray photoelectron spectra (XPS) (Figure S2). The BE of the Re(4f) level in Re@U and Re-Ru@U appears at 41.5 eV, comparable to that of the reported rhenium bipyridine complexes [29]. As for the Ru(3p) level, the BE is located at 462.8 eV in both Ru@U and Re-Ru@U, consistent with reported Ru molecular species [30]. The identical peak shapes and BEs in single metal samples of Re@U/Ru@U and double metal sample of Re-Ru@U suggest the same oxidation states. The structural integrity of molecular complexes within the UiO-66 matrix is monitored by ^{1}H NMR spectra of the digested Re-Ru@U, Re@U and Ru@U with NH_4HCO_3 aqueous solution (Figure S3). In comparison with the pristine ReC_2 and RuC_6 complexes, the featured peaks related to ReC_2 and RuC_6 are observed, respectively, in Re@U and Ru@U, while two sets of peaks simultaneously appear in Re-Ru@U, suggesting the intact molecular complexes were maintained after encapsulation. The aperture diameters of Re-Ru@U and Re@U catalysts based on N_2 adsorption–desorption isotherms (Figure S4) are consistent with the pore sizes of the UiO-66 matrix (~8.0 Å and ~11.0 Å). The incompatibility of the molecular sizes of ReC_2 (12 Å) and RuC_6 (15 Å) to the cage sizes of UiO-66 suggest the defect-introduced integration of molecular complexes into matrix scaffolds. Of note, the surface areas and pore volumes of Re-Ru@U, Re@U and Ru@U (Table S2) decreased to a certain extent when compared with that of the UiO-66 matrix, which should stem from the metallization of Re and Ru complexes.

2.3. Optical Characterization

The optical properties of prepared samples are characterized by UV-Vis diffuse reflection and photoluminescence spectra, as shown in Figure 2. For comparison, the UV-Vis absorption spectra of pristine ReC_2 and RuC_6 complexes dissolved in N,N-dimethylacetamide (DMA) solvent are shown in Figure 2A with dashed lines. The featured absorptions of ReC_2 and RuC_6 complexes, respectively, at 400 and 470 nm are similar to the reported data in references [31–34], ascribed to the metal-to-ligand charge transfers (MLCTs). For the integrated single-metal complex samples, Re@U exhibits an absorption band at ~395 nm, and Ru@U shows an absorption band centred at 470 nm, along with a shoulder at ~550 nm.

As for the co-assembled sample of Re-Ru@U, the absorption feature is the combination of Re@U and Ru@U, with discernible bands at 395, 470 and 550 nm. Notably, no absorption appears in the UiO-66 matrix in the concerned region at 350~650 nm. In the photoluminescence spectra excited by 470 nm (Figure 2B), a strong emission band appears at ~675 nm for the RuC6 complex, associated with the electronic transition from the 3MLCT triplet excited state to ground state. After being integrated into UiO-66 as Ru@U, this emission shifts to 640 nm due to the "luminescence rigidochromism" [35–38]. In contrast, a negligible emission band is observed for the integrated Re@U. Correspondingly, the strong emission of Re-Ru@U is dominated by the RuC_6, with a peak located at ~645 nm.
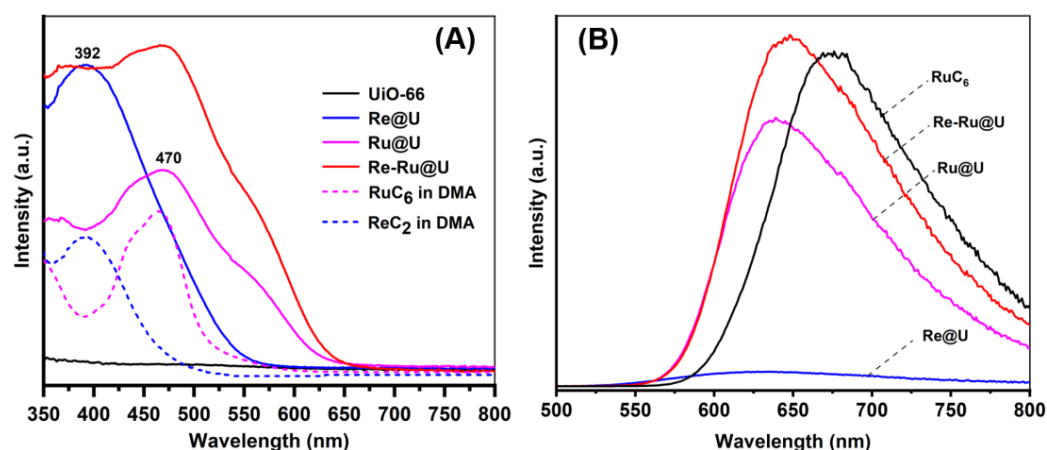

Figure 2. (**A**) UV-Vis diffuse reflection spectra of Re-Ru@U, Re@U and Ru@U and absorption spectra of ReC_2 and RuC_6 complexes dissolved in DMA solvent, (**B**) photoluminescence spectra (λ_{ex} = 470 nm) of RuC_6, Re-Ru@U, Re@U and Ru@U.

2.4. Photocatalytic Performance

Photocatalytic CO_2 reduction is evaluated in a mixed solvent of DMA and triethanolamine (TEOA) (*v*/*v* = 4.5/0.5) with 1,3-dimethyl-2-phenyl-2,3-dihydro-1H-benzimidazole (BIH) as sacrificial agent, irradiating with visible light (λ > 420 nm). Figure 3A gives the CO evolution on different samples along with irradiating time; notably, no H_2 and formic acid were detected during CO_2 reduction. For the Re-Ru@U catalyst, the CO evolution almost linearly increases over time at an initial rate of ~500 μmol/g/h, and the output achieves ~1900 μmol/g within 11 h irradiation. The accumulated turnover number (TON) based on Re centres approaches 15 without obvious deactivation. In contrast, the previously reported dual-metal-complex ReRu-66 sample suffered from quick deactivation after 1.5 h [24], although with a comparable TON value.

In control experiments, the surface-impregnating Re-Ru/U catalyst (brown line), CO generation was only ~45 μmol/g after 6 h reaction. Notably, no CO evolution was detected for Re@U and Ru@U with 3 h irradiation. When introducing an additional RuC_6 complex into solution containing the Re@U catalyst (purple line), 85 μmol/g of CO output was detected. As control, the CO evolutions are further compared with the equivalent amount of ReC_2 and/or RuC_6 complexes dissolved in UiO-66 suspending liquid. In cases of the coexistent ReC_2 and RuC_6 (red line) and the individual ReC_2 (blue line), the CO evolutions are observed with the maximum CO output respective to 1100 μmol/g and 950 μmol/g, followed by quick leave-off after 3 h irradiation. As for the individual RuC_6, no CO is detected. The absence of CO evolution in either light or N_2 atmosphere and the presence of ^{13}CO in GC-MS spectra (Figure S5) of $^{13}CO_2$ isotopic labelling experiment verify the origin of CO from CO_2 photochemical reduction.
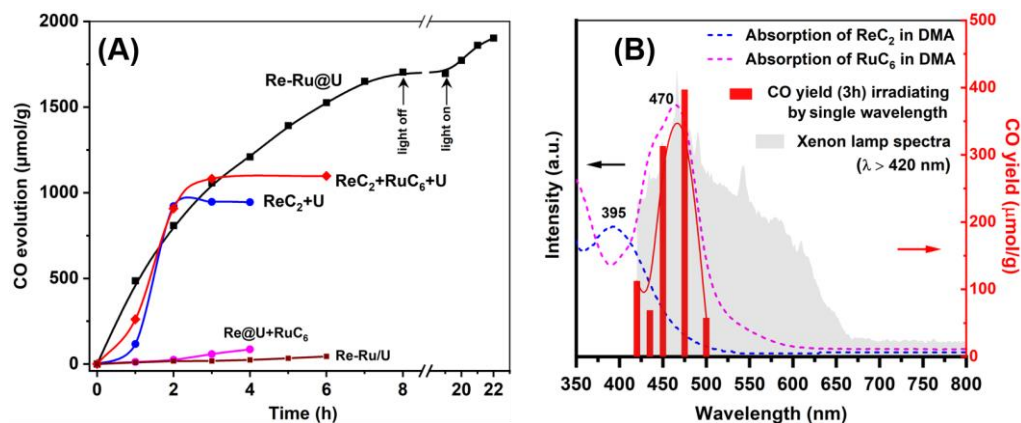
Figure 3. (**A**) CO_2 evolution along with irradiation time in Re-Ru@U catalyst and a serial of control tests. Visible light ($\lambda > 420$ nm) irradiation with 100 mW/cm^2 intensity. (**B**) CO yield (red column) in Re-Ru@U catalyst irradiating with a single wavelength at 420, 435, 450, 475 and 500 nm. The xenon lamp spectra (grey area) used in photocatalytic measurement at 420~800 nm region and the absorption spectra of ReC_2 (blue dash) and RuC_6 (purple dash) complexes dissolved in DMA solvent are added.

Figure 3B gives the CO yield (red column) in the Re-Ru@U catalyst, irradiating with single wavelengths at 420, 435, 450, 475 and 500 nm obtained from a xenon lamp light source with band-pass filters. As a reference, the xenon lamp spectra (grey area) in the 420~800 nm region used in photocatalytic measurement and the absorption spectra of RuC_6 (purple dash) and ReC_2 (blue dash) dissolved in DMA solvent are shown in Figure 3B. When increasing the wavelength from 435 nm to 500 nm, the CO yield increases significantly from ~70 μmol/g (435 nm) to ~310 μmol/g (450 nm) and to ~400 μmol/g (475 nm); further, in the following step, the CO yield sharply declines to ~60 μmol/g (500 nm). This CO evolution tendency is consistent with the absorption peak shape of RuC_6 in DMA, where the maximum absorption at 475 nm causes the highest CO yield, suggesting the light-harvesting function of RuC_6 in the double-metal Re-Ru@U catalyst. When irradiating at 420 nm, an abnormal CO yield of ~110 μmol/g is observed, which is even higher than the activities irradiating at 435 and 500 nm. Based on the facts that the absorption of RuC_6 declines in the short-wavelength direction but the absorption of ReC_2 increases, it is suggested that ReC_2 centres also contribute to light harvesting, in addition to catalytic sites for CO_2 reduction.

2.5. Mechanism Analysis

When comparing the homogeneous system with the heterogeneous systems, the additional introduction of the RuC_6 photosensitizer to ReC_2 (ReC_2 + RuC_6 + U) could not significantly improve the performance of ReC_2, while the performance of co-assembling Re-Ru@U was greatly improved compared with that of Re@U. In order to disclose the activity disparity, the one-electron-reduced (OER) species is measured by electron paramagnetic resonance (EPR) spectra under visible-light irradiation in the presence of TEOA, as shown in Figure 4. Both the heterogenous Re@U and the homogenous ReC_2 with UiO-66 show an EPR signal with a g value of ~2.008; similarly, the Ru@U and the RuC_6 with UiO-66 give a signal with a g value of ~2.002. According to previous reports, these two signals are, respectively, ascribed to ligand-centred radical anions of $[(bpy)Re(CO)_3Cl]^{\bullet-}$ and radical ion complexes of Ru^{II}, whose small deviation from free spin ($g = 2.003$) arises from a small amount of unpaired spin density on the metal atoms [39,40]. As for the co-assembly of Re-Ru@U, the simultaneous appearance of two signals with g values of 2.0076 and 2.003 indicates the co-existence of dual ligand-centred radical species without interference with each other; that is, Re and Ru centres could be separately one-electron reduced during irradiation in the presence of an electron sacrificial reagent. This result is consistent with

the above deduction that ReC_2 centres bear double functions in the Re-Ru@U catalyst to harvest light and catalyse conversion.
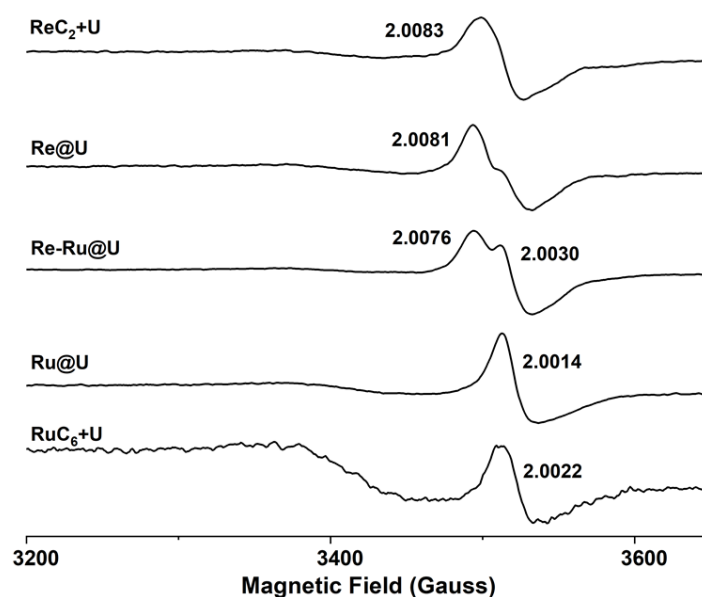
Figure 4. The room temperature EPR spectra of Re-Ru@U, Re@U, Ru@U and the mixtures of ReC_2/RuC_6 complexes with UiO-66 under visible-light irradiation. The powder samples used in EPR test were immersed in DMA/TEOA (5/1) solvent with visible light irradiation.

The two-electron conversion of CO_2 in the Re complex involves a photochemical cycle where OER species of $Re^I(bipy^{\bullet-})(CO)_3X$ are generated and a sequence dark cycle in which Re-CO_2 intermediate species acquire the second electron to generate CO [41], where the second electron is indispensable for CO evolution. In a homogenous ReC_2 system, the Re complex takes on the duel identities of a photosensitizer and an active catalyst for CO_2 conversion to CO, and the second electron could be easily acquired from the other Re-based OER species, with a double-molecule mechanism accompanying the irreversible dimerization inactivation [41]. The slight increase in CO output in a homogenous ReC_2 and RuC_6 co-existent system, compared with single ReC_2, suggests that ReC_2 dominates in CO evolution suffered from the quick inactivation and a tiny contribution from RuC_6. As for heterogenous Re@U featuring highly isolated Re centres, the OER species is detected but with no CO generation, suggesting a lack of the source of the second electron. Furthermore, trace amounts of CO appearing in the presence of additional RuC_6 indicate the limited electron transfer between RuC_6 and Re@U. On the contrary, the coexistence of dual-radical species in Re-Ru@U corresponds to sustained and steady CO evolution. The sharp contrast in activity of Re@U, Re@U + RuC_6 and Re-Ru@U prompts us to presume that the co-existent Ru-based OER species within UiO-66 supply the second electron to assist the Re-centred catalytic cycle.

This presumption is evidenced by the comparison of recycled Re-Ru@U with pristine Re-Ru@U. In the IR spectra (Figure 5A), the three featured IR peaks retained in the recycled sample experienced several wavenumber shifts to a lower-energy direction. In view of the sensitivity of carbonyl IR bands to electron density in the central rhenium atom [15,42–44], these shifts suggest an increase in electron densities on Re centres partly. In XPS results, the BE of Ru $3d_{5/2}$ (overlapping with C 1s) underwent a 0.3 eV shift from 281.2 to 281.5 eV after reaction (Figure 5B), indicating a decrease in electron density at Ru centres. Therefore, electron transfer occurs from Ru to Re centres during the photocatalytic process, although the tiny change in electron density on Re centres is only monitored by IR and not XPS.
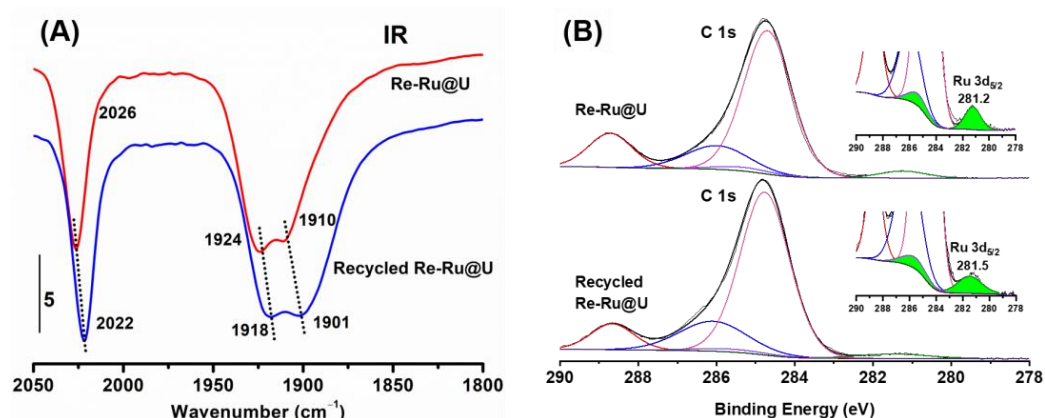
Figure 5. (**A**) IR and (**B**) XPS spectra of C 1s/Ru 3d in Re-Ru@U before and after photocatalytic reaction. The inset in (**B**) is enlarged spectra to show Ru 3d clearly.

The photocatalytic CO_2 reduction on the Re-Ru@U catalyst is briefly illustrated in Figure 6, where both Re and Ru centres within UiO-66 are photoexcited and then reductive quenching by sacrificial reagents to generate OER species simultaneously. In the following step, the evolved Re-based intermediates further acquire the second electron from Ru centres to produce CO, sustainably and stably. The chemical stability of the Re-Ru@U catalyst was studied by the comparison of recycled Re-Ru@U after photocatalysis to the pristine Re-Ru@U (Figure S5). The consistent diffraction patterns in PXRD for Re-Ru@U before and after reaction, the comparable absorption features in UV-Vis spectra and the retention of BE location for Re(4f) level are observed, which suggests improved stability for the heterogenous Re and Ru complexes within the UiO-66 matrix to survive under the harsh reaction condition.
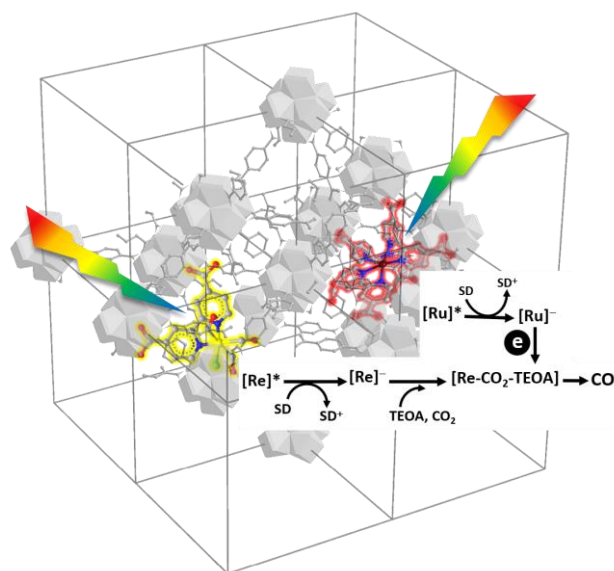
Figure 6. The functional illustration of ReC_2 and RuC_6 complexes in Re-Ru@U catalysts during photocatalytic CO_2 reduction in the presence of TEOA/BIH, irradiating by visible light ($\lambda > 420$ nm). ([Re]* and [Ru]* represent the light-induced excited states of Re and Ru complexes).

3. Materials and Methods

3.1. Chemicals

Chemical reagents used were all purchased without further purification. All reagents were obtained from commercial sources (Alfa Aesar (Shanghai, China), Bidepharm (Shanghai, China), Macklin (Shanghai, China), Aladdin (Shanghai, China)) and were used without

further purification. Specifically, we used the following: p-Phthalic acid (PTA, 95%), 2,2′-Bipyridine-4,4′-dicarboxylic acid (H$_2$BPYDC), Zirconium(IV) propoxide solution (70 wt.% in 1-propanol), acetic acid, N, N-dimethylformamide (DMF, 99.9%), N, N-Dimethylacetamide (DMA, 99.9%), toluene (AR), Iodomethane (98%), and 2-Phenylbenzimidazole (>98%).

3.2. Synthesis

3.2.1. Synthesis of fac-[Re^I(dcbpy)(CO)$_3$Cl]

Re^I(dcbpy)(CO)$_3$Cl was synthesized in a pure aqueous system, similar to a previous report [45]. Re(CO)$_5$Cl and 2,2′-Bipyridine-4,4′-dicarboxylic acid (H$_2$BPYDC, 0.55 mmol) were added to mixed solvent of methanol (20 mL) and toluene(50 mL). The solution was refluxed under N$_2$ for 2 h until it turned orange red and then fully filtered to remove unreacted raw materials. The system was cooled to room temperature, and the solvent was subsequently removed under reduced pressure. The product was dried under vacuum at 60 °C to give deep-orange powders.

3.2.2. Synthesis of UiO-66

UiO-66 was synthesized by a room-temperature method from the literature [26]. To a 20 mL scintillation vial, 71 µL of a 70% zirconium propoxide [Zr(OnPr)$_4$] solution was added in 1-propanol (0.158 mmol), 7 mL of DMF, and 4 mL of acetic acid (70 mmol). The solution was placed on a heating plate and heated at 130 °C, denoted as Zr-oxo solution. PTA (0.45 mmol) was added into above solution and stirred at 200 rpm to obtain white precipitate. Then, the white precipitate was separated, washed several times with DMF and solvent exchanged with absolute methanol. The final products were heated at 60 °C in a vacuum oven overnight before being analyzed, denoted as UiO-66.

3.2.3. Synthesis of Re@U

Re(4,4′-dcbpy)(CO)$_3$Cl was dissolved in Zr-oxo solution. After stirring for 1 h, PTA (0.1 mmol) was added to the mixed solution. After ultrasonic dispersion for 30 s, the mixture was placed at 25 °C and stirred slowly for 18 h. The yellow powders were collected by centrifugation and washed repeatedly twice in DMF, and absolute methanol was then vacuum dried at 60 °C overnight. The obtained powders were recorded as Re@U.

3.2.4. Synthesis of Ru@U

[Ru(dcbpy)$_3$]Cl$_2$ was dissolved in Zr-oxo solution. After stirring for 1 h, PTA (0.1 mmol) was added to the mixed solution. The subsequent synthesis method was consistent with the synthesis of Re@U. The obtained powders were recorded as Ru@U.

3.2.5. Synthesis of Re-Ru@U

Re(4,4′-dcbpy)(CO)$_3$Cl and [Ru(dcbpy)$_3$]Cl$_2$ were dissolved simultaneously in Zr-oxo solution. After stirring for 1 h, PTA (0.1 mmol) was added to the mixed solution. The subsequent synthesis method was consistent with the synthesis of Re@U. The obtained powders were recorded as Re-Ru@U. The metal content of the material was determined by ICP-AES, as shown in the Supplementary Materials.

3.2.6. Synthesis of Re-Ru/U

The equivalent Re(4,4′-dcbpy)(CO)$_3$Cl and [Ru(dcbpy)$_3$]Cl$_2$ to Re-Ru@U were dissolved simultaneously in solvent and then UiO-66 was added. After ultrasonic dispersion followed by stirring for 3 h, the solvent was withdrawn from the above solution via rotary evaporation. The product was dried at 80 °C under vacuum overnight to obtain the powder sample, denoted as Re-Ru/U.

3.3. Characterization

Transmission electron microscopy (TEM), high-angle annular dark-field scanning transmission electron microscopy (HAADF-STEM) and EDX mapping images were per-

formed on an Aberration Corrected Microscope (JEOL ARM-200F, Tokyo, Japan) equipped with energy-dispersive X-ray spectrometer operating at 200 kV with the samples deposited on carbon-coated copper grids. UV-vis absorption spectra were tested on a Shimadzu(Kyoto, Japan) UV-3600 UV-Vis spectrometer with measurement range from 200 to 800 nm. Powder XRD patterns were recorded at room temperature on a Smart-Lab diffractometer (D8 Advance Bruker, Rheinstetten, Germany) using Cu Kα radiation (λ = 1.54059 Å) at 40 kV and 30 mA. Fourier-transform infrared spectroscopy (FTIR) spectra were collected on a VERTEX 70 (Bruker, Rheinstetten, Germany) equipped with a Diamond ATR (attenuated total reflectance) accessory in the wavenumber range of 4000–400 cm^{-1}. XPS investigation was performed in a K-alpha spectrometer (Thermo Fisher Scientific, Waltham, MA, USA) using a monochromatic Al Kα X-ray source (1486.7 eV, 400 μm spot size). All spectra were referenced to the C 1s peak at 284.8 eV binding energy (C–H). ICP spectroscopy was conducted on a Spectro Ciros Vision ICP-AES spectrometer (Kleve, Germany) equipped with vacuum optics, covering a spectral range from 175 to 777 nm; plasma power 1300 w; coolant flow 15.00 L/min; auxiliary flow 0.80 L/min; nebulizer 0.70 L/min. The room steady-state emission spectra and emission lifetime were measured by photoluminescence spectrometer (Edinburgh Instruments Ltd. FLS980, Livingston, Scotland) equipped with a continuous Xe900 Xenon lamp. ^{1}H NMR spectra were recorded on Bruker AVANCE III 400 (400 MHz, Rheinstetten, Germany). Chemical shifts were quoted in parts per million (ppm) referenced to the appropriate solvent peak. N$_2$ adsorption and desorption isotherms were measured with a JW-BK200 (Beijing JWGB instrument Co., Ltd. JW-BK 200, Beijing, China).

3.4. EPR Test

The EPR spectra were carried out in ESR spectrometer system, (JEOL, JES-FA200, Tokyo, Japan) at room temperature. The powder samples of Re@U, Ru@U and Re-Ru@U were immersed. For ReC$_2$ and RuC$_6$ complexes, they were, respectively, dissolved into DMA/TEOA (5/1) solvent and then added to UiO-66 matrix powder. During measurement, all samples were irradiated by the xenon lamp light source with visible light (λ > 420 nm).

3.5. Photocatalytic Test

Photocatalytic CO$_2$ reduction is evaluated in a 50 mL closed glass vial with magnetic stirring. A mixed solvent of DMA and TEOA (v/v = 4.5/0.5) was used with 1,3-dimethyl-2-phenyl-2,3-dihydro-1H-benzimidazole (BIH) as sacrificial agent. In detail, 1 mg catalyst was dispersed in DMA solvent (V$_{total}$ = 5 mL), irradiating with visible light (λ > 420 nm). The gaseous products were analyzed via Shimadzu (Kyoto, Japan) GC-2014 gas chromatography equipped with Shimadzu Molecular Sieve 13X 80/100 3.2 × 2.1 mm × 3.0 m and Porapak N 3.2 × 2.1 mm × 2.0 m columns. A thermal conductivity detector (TCD) was used to detect H$_2$, and a flame ionization detector (FID) with a methanizer was used to detect CO and other hydrocarbons. Nitrogen was used as the carrier gas. ^{13}C isotopic labelling experiments were carried out in a ^{13}CO$_2$ atmosphere, and gas products were detected by GC-MS (Agilent 7890A5975C, Shanghai, China)).

4. Conclusions

The co-encapsulation of ReC$_2$ and RuC$_6$ metal complexes into the UiO-66 matrix makes ReC$_2$ and RuC$_6$, separated physically, work as the light-harvesting centres individually, without mutual interference, meanwhile endowing them with electron communication after photoinduced single-electron reduction. This work demonstrates an alternative strategy to integrate bimetallic or multimetallic centres into MOF scaffolds to fulfil the unexpected multiple functions in the photocatalytic field.

Supplementary Materials: The following supporting information can be downloaded at: https://www.mdpi.com/article/10.3390/catal13121510/s1, Table S1: The summary of feeding quantity and ICP content of Re-Ru@U and the corresponding CO yield; Figure S1: (A) PXRD and (B) IR spectra of ReC$_2$, RuC$_6$, Re-Ru@U, Re@U, Ru@U and UiO-66; Figure S2: XPS binding energy of (A) Re 4f and (B) Ru 3p in samples of Re@U, Ru@U and Re-Ru@U; Figure S3: ^{1}H NMR (D$_2$O-DMSO-d^6) spectra of pristine ReC$_2$ and RuC$_6$ complexes and the digested samples of Re-Ru@U, Re@U, Ru@U and UiO-66; Figure S4: (A) 77K N$_2$ adsorption and desorption isothermal curves and (B) cumulative pore size profiles for different assembled catalysts; Table S2: Porous structure analysis; Figure S5:The product analysis by GC/MS chromatograms for photocatalytic CO$_2$ reduction in ^{13}CO$_2$-saturated DMA-TEOA (v/v = 9:1) solution containing 1 mg catalyst and 28 mg BIH; Figure S6: (A) XRD patterns, (B) UV-Vis spectra and (C) Re 4f XPS spectra of Re-Ru@U and recycled Re-Ru@U samples; Table S3: CO$_2$ conversion performances of Re and Ru complexes incorporated into different MOFs [13,23,24,27,46,47].

Author Contributions: Conceptualization, Z.S. and J.S.; methodology, Z.S. and B.Y.; validation, J.F. and M.Z.; formal analysis, J.F.; investigation, Z.S.; data curation, Z.S.; writing—original draft preparation, Z.S. and B.Y.; writing—review and editing, B.Y. and J.S.; visualization, X.L.; supervision and funding acquisition, J.S. All authors have read and agreed to the published version of the manuscript.

Data Availability Statement: All research data are included in this article.

Conflicts of Interest: The authors declare no conflict of interest.

References

1. Yamazaki, Y.; Miyaji, M.; Ishitani, O. Utilization of Low-Concentration CO$_2$ with Molecular Catalysts Assisted by CO$_2$-Capturing Ability of Catalysts, Additives, or Reaction Media. *J. Am. Chem. Soc.* **2022**, *144*, 6640–6660. [CrossRef] [PubMed]
2. Khalil, M.; Gunlazuardi, J.; Ivandini, T.A.; Umar, A. Photocatalytic conversion of CO$_2$ using earth-abundant catalysts: A review on mechanism and catalytic performance. *Renew. Sustain. Energy Rev.* **2019**, *113*, 109246. [CrossRef]
3. Lehn, J.M.; Ziessel, R. Photochemical generation of carbon monoxide and hydrogen by reduction of carbon dioxide and water under visible light irradiation. *Proc. Nati. Acad. Sci. USA* **1982**, *79*, 701–704. [CrossRef] [PubMed]
4. Bourrez, M.; Molton, F.; Chardon-Noblat, S.; Deronzier, A. [Mn(bipyridyl)(CO)$_3$Br]: An abundant metal carbonyl complex as efficient electrocatalyst for CO$_2$ reduction. *Angew. Chem. Int. Ed. Engl.* **2011**, *50*, 9903–9906. [CrossRef] [PubMed]
5. Clark, M.L.; Grice, K.A.; Moore, C.E.; Rheingold, A.L.; Kubiak, C.P. Electrocatalytic CO$_2$ reduction by M(bpy-R)(CO)$_4$ (M = Mo, W; R = H, tBu) complexes. Electrochemical, spectroscopic, and computational studies and comparison with group 7 catalysts. *Chem. Sci.* **2014**, *5*, 1894–1900. [CrossRef]
6. Yamazaki, Y.; Takeda, H.; Ishitani, O. Photocatalytic reduction of CO$_2$ using metal complexes. *J. Photochem. Photobiol. C: Photochem. Rev.* **2015**, *25*, 106–137. [CrossRef]
7. Morimoto, T.; Nishiura, C.; Tanaka, M.; Rohacova, J.; Nakagawa, Y.; Funada, Y.; Koike, K.; Yamamoto, Y.; Shishido, S.; Kojima, T.; et al. Ring-Shaped Re(I) Multinuclear Complexes with Unique Photofunctional Properties. *J. Am. Chem. Soc.* **2013**, *135*, 13266–13269. [CrossRef] [PubMed]
8. Umemoto, A.; Yamazaki, Y.; Saito, D.; Tamaki, Y.; Ishitani, O. Synthesis of a Novel Re(I)-Ru(II)-Re(I) Trinuclear Complex as an Effective Photocatalyst for CO$_2$ Reduction. *Bull. Chem. Soc. Jpn.* **2020**, *93*, 127–137. [CrossRef]
9. Cancelliere, A.M.; Puntoriero, F.; Serroni, S.; Campagna, S.; Tamaki, Y.; Saito, D.; Ishitani, O. Efficient trinuclear Ru(II)-Re(I) supramolecular photocatalysts for CO$_2$ reduction based on a new tris-chelating bridging ligand built around a central aromatic ring. *Chem. Sci.* **2020**, *11*, 1556–1563. [CrossRef]
10. Ohkubo, K.; Yamazaki, Y.; Nakashima, T.; Tamaki, Y.; Koike, K.; Ishitani, O. Photocatalyses of Ru(II)–Re(I) binuclear complexes connected through two ethylene chains for CO$_2$ reduction. *J. Catal.* **2016**, *343*, 278–289. [CrossRef]
11. Maeda, K. Metal-Complex/Semiconductor Hybrid Photocatalysts and Photoelectrodes for CO$_2$ Reduction Driven by Visible Light. *Adv. Mater.* **2019**, *31*, e1808205. [CrossRef] [PubMed]
12. Hawecker, J.; Lehn, J.-M.; Ziessel, R. Photochemical and Electrochemical Reduction of Carbon Dioxide to Carbon Monoxide Mediated by (2,2′-Bipyridine)tricarbonylchlororhenium(I) and Related Complexes as Homogeneous Catalysts. *Helv. Chim. Acta* **1986**, *69*, 1990–2012. [CrossRef]
13. Karmakar, S.; Barman, S.; Rahimi, F.A.; Maji, T.K. Covalent grafting of molecular photosensitizer and catalyst on MOF-808: Effect of pore confinement toward visible light-driven CO$_2$ reduction in water. *Energy Environ. Sci.* **2021**, *14*, 2429–2440. [CrossRef]
14. Shi, J.; Su, Z.; Li, X.; Feng, J.; Men, C. Impacts of host-guest assembly on photophysical and photocatalytic properties of heterogenized molecular photosensitizer and catalysts. *J. Mater. Chem. A* **2023**, *11*, 6646–6658. [CrossRef]
15. Huang, R.; Peng, Y.; Wang, C.; Shi, Z.; Lin, W. A rhenium-functionalized metal-organic framework as a single-site catalyst for photochemical reduction of carbon dioxide. *Eur. J. Inorg. Chem.* **2016**, *2016*, 4358–4362. [CrossRef]

16. Wang, C.; Xie, Z.; deKrafft, K.E.; Lin, W. Doping Metal–Organic Frameworks for Water Oxidation, Carbon Dioxide Reduction, and Organic Photocatalysis. *J. Am. Chem. Soc.* **2011**, *133*, 13445–13454. [CrossRef]

17. Burgun, A.; Coghlan, C.J.; Huang, D.M.; Chen, W.; Horike, S.; Kitagawa, S.; Alvino, J.F.; Metha, G.F.; Sumby, C.J.; Doonan, C.J. Mapping-Out Catalytic Processes in a Metal–Organic Framework with Single-Crystal X-ray Crystallography. *Angew. Chem. Int. Ed.* **2017**, *56*, 8412–8416. [CrossRef]

18. Peralta, R.A.; Huxley, M.T.; Evans, J.D.; Fallon, T.; Cao, H.; He, M.; Zhao, X.S.; Agnoli, S.; Sumby, C.J.; Doonan, C.J. Highly Active Gas Phase Organometallic Catalysis Supported Within Metal–Organic Framework Pores. *J. Am. Chem. Soc.* **2020**, *142*, 13533–13543. [CrossRef]

19. Luo, Y.-C.; Chu, K.-L.; Shi, J.-Y.; Wu, D.-J.; Wang, X.-D.; Mayor, M.; Su, C.-Y. Heterogenization of Photochemical Molecular Devices: Embedding a Metal-Organic Cage into a ZIF-8-Derived Matrix To Promote Proton and Electron Transfer. *J. Am. Chem. Soc.* **2019**, *141*, 13057–13065. [CrossRef]

20. Luo, Y.; Fan, S.; Yu, W.; Wu, Z.; Cullen, D.A.; Liang, C.; Shi, J.; Su, C. Fabrication of $Au_{25}(SG)_{18}$-ZIF-8 Nanocomposites: A Facile Strategy to Position $Au_{25}(SG)_{18}$ Nanoclusters Inside and Outside ZIF-8. *Adv. Mater.* **2018**, *30*, 1704576. [CrossRef]

21. Wu, D.-J.; Luo, Y.; Li, X.; Su, Z.-F.; Shi, J.-Y.; Su, C.-Y. Revisiting the Environment Effect on Mass Transfer for Heterogenized Pd6Ru8 Metal-Organic Cage Photocatalyst Confined within 3D Matrix. *Chem.–A Eur. J.* **2022**, *28*, e202200310. [CrossRef] [PubMed]

22. Su, Z.; Luo, Y.; Shi, J.; Feng, J.; Li, X.; Zhang, J.; Su, C. Manipulating the Reaction Pathway of CO_2 Photoreduction via the Microenvironment of a Re Molecular Catalyst. *J. Phys. Chem. Lett.* **2023**, *14*, 3208–3215. [CrossRef] [PubMed]

23. Deng, X.; Albero, J.; Xu, L.; García, H.; Li, Z. Construction of a Stable Ru–Re Hybrid System Based on Multifunctional MOF-253 for Efficient Photocatalytic CO_2 Reduction. *Inorg. Chem.* **2018**, *57*, 8276–8286. [CrossRef] [PubMed]

24. Stanley, P.M.; Haimerl, J.; Thomas, C.; Urstoeger, A.; Schuster, M.; Shustova, N.B.; Casini, A.; Rieger, B.; Warnan, J.; Fischer, R.A. Host–Guest Interactions in a Metal–Organic Framework Isoreticular Series for Molecular Photocatalytic CO_2 Reduction. *Angew. Chem. Int. Ed.* **2021**, *60*, 17854–17860. [CrossRef]

25. Ragon, F.; Campo, B.; Yang, Q.; Martineau, C.; Wiersum, A.D.; Lago, A.; Guillerm, V.; Hemsley, C.; Eubank, J.F.; Vishnuvarthan, M.; et al. Acid-functionalized UiO-66(Zr) MOFs and their evolution after intra-framework cross-linking: Structural features and sorption properties. *J. Mater. Chem. A* **2015**, *3*, 3294–3309. [CrossRef]

26. DeStefano, M.R.; Islamoglu, T.; Garibay, S.J.; Hupp, J.T.; Farha, O.K. Room-Temperature Synthesis of UiO-66 and Thermal Modulation of Densities of Defect Sites. *Chem. Mater.* **2017**, *29*, 1357–1361. [CrossRef]

27. Waki, M.; Yamanaka, K.I.; Shirai, S.; Maegawa, Y.; Goto, Y.; Yamada, Y.; Inagaki, S. Re(bpy)(CO)3 Cl Immobilized on Bipyridine-Periodic Mesoporous Organosilica for Photocatalytic CO_2 Reduction. *Chemistry* **2018**, *24*, 3846–3853. [CrossRef] [PubMed]

28. Abdellah, M.; El-Zohry, A.M.; Antila, L.J.; Windle, C.D.; Reisner, E.; Hammarstrom, L. Time-Resolved IR Spectroscopy Reveals a Mechanism with TiO_2 as a Reversible Electron Acceptor in a $TiO_2−Re$ Catalyst System for CO_2 Photoreduction. *J. Am. Chem. Soc.* **2017**, *139*, 1226–1232. [CrossRef]

29. Johnson, E.M.; Haiges, R.; Marinescu, S.C. Covalent-Organic Frameworks Composed of Rhenium Bipyridine and Metal Porphyrins: Designing Heterobimetallic Frameworks with Two Distinct Metal Sites. *ACS Appl. Mater. Interfaces* **2018**, *10*, 37919–37927. [CrossRef]

30. Hao, M.; Xie, Y.; Liu, X.; Chen, Z.; Yang, H.; Waterhouse, G.I.N.; Ma, S.; Wang, X. Modulating Uranium Extraction Performance of Multivariate Covalent Organic Frameworks through Donor-Acceptor Linkers and Amidoxime Nanotraps. *JACS Au* **2023**, *3*, 239–251. [CrossRef]

31. Ishida, H.; Fujiki, K.; Ohba, T.; Ohkubo, K.; Tanaka, K.; Terada, T.; Tanaka, T. Ligand effects of ruthenium 2,2′-bipyridine and 1,10-phenanthroline complexes on the electrochemical reduction of CO_2. *J. Chem. Soc. Dalton Trans.* **1990**, *7*, 2155–2160. [CrossRef]

32. Voyame, P.; Toghill, K.E.; Méndez, M.A.; Girault, H.H. Photoreduction of CO_2 Using $[Ru(bpy)_2(CO)L]^{n+}$ Catalysts in Biphasic Solution/Supercritical CO_2 Systems. *Inorg. Chem.* **2013**, *52*, 10949–10957. [CrossRef] [PubMed]

33. Stufkens, D.J. The Remarkable Properties of α-Diimine Rhenium Tricarbonyl Complexes in Their Metal-to-Ligand Charge-Transfer (MLCT) Excited States. *Comments Inorg. Chem.* **1992**, *13*, 359–385. [CrossRef]

34. Ishida, H.; Tanaka, H.; Tanaka, K.; Tanaka, T. Selective formation of $HCOO^−$ in the electrochemical CO_2 reduction catalysed by $[Ru(bpy)_2(CO)_2]^{2+}$(bpy = 2,2′-bipyridine). *J. Chem. Soc. Chem. Commun.* **1987**, *2*, 131–132. [CrossRef]

35. Faustino, L.A.; Souza, B.L.; Nunes, B.N.; Duong, A.-T.; Sieland, F.; Bahnemann, D.W.; Patrocinio, A.O.T. Photocatalytic CO_2 Reduction by Re(I) Polypyridyl Complexes Immobilized on Niobates Nanoscrolls. *ACS Sustain. Chem. Eng.* **2018**, *6*, 6073–6083. [CrossRef]

36. Polo, A.S.; Itokazu, M.K.; Murakami Iha, N.Y. Photoinduced luminescence of *fac*-[Re(CO)3(phen)(stpy)]+ in CH3CN and PMMA. *J. Photochem. Photobiol. A: Chem.* **2006**, *181*, 73–78. [CrossRef]

37. Lakowicz, J.R. *Principles of Fluorescence Spectroscopy*, 3rd ed.; Springer Science+Business Media, LLC: New York, NY, USA, 2006.

38. Patrocinio, A.O.; Frin, K.P.; Murakami Iha, N.Y. Solid state molecular device based on a rhenium(I) polypyridyl complex immobilized on TiO_2 films. *Inorg. Chem.* **2013**, *52*, 5889–5896. [CrossRef] [PubMed]

39. Poppe, J.; Kaim, W.; Altabef, A.B.; Katz, N.E. EPR characteristics of radical complexes with coordinated ammineruthenium(II) fragments. Evidence for the metal-to-ligand charge transfer (MLCT) nature of the low-lying excited states in precursor complexes. *J. Chem. Soc. Perkin Trans. 2* **1993**, *11*, 2105–2108. [CrossRef]

40. Scheiring, T.; Klein, A.; Kaim, W. EPR study of paramagnetic rhenium(I) complexes (bpy>>·>>−>>) Re(CO)3X relevant to the mechanism of electrocatalytic CO_2 reduction[†]. *J. Chem. Soc. Perkin Trans. 2* **1997**, *12*, 2569–2572. [CrossRef]

41. Kuramochi, Y.; Ishitani, O.; Ishida, H. Reaction mechanisms of catalytic photochemical CO_2 reduction using Re(I) and Ru(II) complexes. *Coord. Chem. Rev.* **2018**, *373*, 333–356. [CrossRef]

42. Takeda, H.; Koike, K.; Morimoto, T.; Inumaru, H.; Ishitani, O. Photochemistry and photocatalysis of rhenium(I) diimine complexes. In *Advances in Inorganic Chemistry*; Eldik, R.V., Stochel, G., Eds.; Academic Press: Cambridge, MA, USA, 2011; Volume 63, pp. 137–186.

43. Kuramochi, Y.; Sekine, M.; Kitamura, K.; Maegawa, Y.; Goto, Y.; Shirai, S.; Inagaki, S.; Ishida, H. Photocatalytic CO_2 Reduction by Periodic Mesoporous Organosilica (PMO) Containing Two Different Ruthenium Complexes as Photosensitizing and Catalytic Sites. *Chem.–A Eur. J.* **2017**, *23*, 10301–10309. [CrossRef] [PubMed]

44. Ettedgui, J.; Diskin-Posner, Y.; Weiner, L.; Neumann, R. Photoreduction of Carbon Dioxide to Carbon Monoxide with Hydrogen Catalyzed by a Rhenium(I) Phenanthroline−Polyoxometalate Hybrid Complex. *J. Am. Chem. Soc.* **2011**, *133*, 188–190. [CrossRef] [PubMed]

45. Juris, A.; Campagna, S.; Bidd, I.; Lehn, J.M.; Ziessel, R. Synthesis and photophysical and electrochemical properties of new halotricarbonyl(polypyridine)rhenium(I) complexes. *Inorg. Chem.* **1988**, *27*, 4007–4011. [CrossRef]

46. Stanley, P.M.; Thomas, C.; Thyrhaug, E.; Urstoeger, A.; Schuster, M.; Hauer, J.; Rieger, B.; Warnan, J.; Fischer, R.A. Entrapped Molecular Photocatalyst and Photosensitizer in Metal–Organic Framework Nanoreactors for Enhanced Solar CO_2 Reduction. *ACS Catalysis* **2021**, *11*, 871–882. [CrossRef]

47. Stanley, P.M.; Parkulab, M.; Rieger, B.; Warnan, J.; Fischer, R.A. Understanding entrapped molecular photosystem and metal-organic framework synergy for improved solar fuel production. *Faraday Discuss* **2021**, *231*, 281–297. [CrossRef]